JOURNAL OF THE KOREAN ASTRONOMICAL SOCIETY
41: 39 ~ 47, 2008 April

CAPABILITY OF THE FAST IMAGING SOLAR SPECTROGRAPH ON NST/BBSO FOR OBSERVING FILAMENTS/PROMINENCES AT THE SPECTRAL LINES Hα, Ca II 8542, AND Ca II K

KWANGSU AHN[1], JONGCHUL CHAE[1], HYUNG-MIN PARK[2,3], JAKYOUNG NAH[2], YOUNG-DEUK PARK[2], BI-HO JANG[2], AND YONG-JAE MOON[4]
[1] Department of Physics and Astronomy, Seoul National University, Seoul 151-742, Korea
E-mail: ksahn@astro.snu.ac.kr
[2] Korea Astronomy and Space Science Institute, Korea
[3] Department of Astronomy and Space Science, Chungnam National University, Korea
[4] Department of Astronomy and Space Science, Kyunghee University, Korea
(Received: March 4, 2008; Accepted: April 16, 2008)

ABSTRACT

Spectral line profiles of filaments/prominences to be observed by the Fast Imaging Solar Spectrograph (FISS) are studied. The main spectral lines of interests are Hα, Ca II 8542, and Ca II K. FISS has a high spectral resolving power of 2×10^5, and supports simultaneous dual-band recording. This instrument will be installed at the 1.6m New Solar Telescope (NST) of Big Bear Solar Observatory, which has a high spatial resolution of 0.065″ at 500nm. Adopting the cloud model of radiative transfer and using the model parameters inferred from pre-existing observations, we have simulated a set of spectral profiles of the lines that are emitted by a filament on the disk or a prominence at the limb. Taking into account the parameters of the instrument, we have estimated the photon count to be recorded by the CCD cameras, the signal-to-noise ratios, and so on. We have also found that FISS is suitable for the study of multi-velocity threads in filaments if the spectral profiles of Ca II lines are recorded together with Hα lines.

Key words : instruments — sun:filaments/prominences — sun:fine threads — spectral profiles

I. INTRODUCTION

Filaments/prominences are known to be composed of fine threads. Because of the limitation in the spatial and spectral resolution of observing instruments, it has been difficult to find out physical parameters of the threads in detail up to now. The New Solar Telescope (NST) under construction at Big Bear Solar Observatory is to have a high spatial resolution of up to 0.065″ at 500nm with the aid of adaptive optics (Denker et al. 2006, Goode et al. 2003). On the other hand, the Fast Imaging Solar Spectrograph (FISS) under development as one of the post-focus instruments of NST is to have a high spectral resolution. Therefore, we expect the FISS on NST will yield data of high spatial and high spectral resolutions that are useful for the study of filaments/prominences.

The solar astronomy group in Seoul National University is developing the FISS in collaboration with Solar and Space Weather Group in Korean Astronomy and Space Science Institute. FISS uses an Echelle grating as the main disperser. A section of a paraboloid mirror of 1.5m focal length is used as both a collimator and an imager. The expected resolving power is 2×10^5. Spectral lines at two different spectral bands are recorded simultaneously with two identical CCD cameras. If spectral lines emitted by different atomic species are recorded, it is useful not only for discriminating the thermal broadening and non-thermal broadening, but also for inducing physical parameters such as temperature and number density. For example, Zhang et al. (1987) used Hα and Ca II K lines to deduced the two-dimensional distributions of physical parameters in prominences. Zhang et al. (1987) used multi-line spectra to obtain the non-LTE semi-empirical model of a prominence. These results demonstrate clearly the importance of multi-line observations.

Many studies have been performed to analyze structures of filaments/prominences (Stellmacher & Wiehr 1973, Engvold et al. 1978, Kubota 1980 and so on). Engvold et al.(1978) suggested that prominences may consist of multiple components. For a couple of reasons, we expect that our new instrument will provide many valuable data on the fine structure of filaments/prominences so that we may reveal their physical nature. Firstly, it will produce data with high spatial and spectral resolution. It will also record simultaneously two spectral bands.

Since low spatial and spectral resolution cause overlapping of threads, it has been difficult to resolve threads individually. Thus, unless their bulk veloci-

Corresponding Author: K. Ahn

ties exceed the limit of Gaussian distribution, several threads could be bundled as a 'velocity thread', which has similar motions. Each of the threads constituting a velocity thread is called as a 'density thread'. Each density thread is characterized by density and temperature (Mein & Mein 1991).

The purpose of this study is to simulate spectral profiles of lines formed in filaments/prominences. The spectral lines of our interest are Hα, Ca II 8542, and Ca II K. In addition, we have considered instrumental specifications of FISS so as to find out the capability of FISS in these lines. Finally, we point out the advantages of Ca II lines over Hα for distinguishing each velocity thread component from spectral line profiles.

II. CLOUD MODEL

To calculate the intensities of spectral lines formed in filaments/prominences, we have applied a simple radiative transfer model which regards a filament/prominence as a cloud (Beckers 1964). Even though many studies regarded the source function of filaments/prominences as a variable function of optical depth (Tziotziou et al. 2001, Zhang et al. 1987, Zhang & Fang 1987), we have assumed that the source function is invariant with optical depth for simplicity. This assumption is known to be valid unless the layer is optically thick or large velocity gradients exist (e.g., Tziotziou 2007).

From the radiative transfer equation

$$\frac{dI_\lambda}{d\tau_\lambda} = I_\lambda - S_\lambda, \tag{1}$$

we obtain the expression of the observed intensity I_λ^{out},

$$I_\lambda^{out} = I_\lambda^{in} e^{-\tau_\lambda} + S_\lambda(1 - e^{-\tau_\lambda}). \tag{2}$$

Here, I_λ^{in} is the incident intensity from the photosphere.

It is convenient to define contrast C_λ with respect to the intensity I_λ^{in}

$$C_\lambda \equiv \frac{I_\lambda^{out} - I_\lambda^{in}}{I_\lambda^{in}} = \left(\frac{S_\lambda}{I_c}\frac{I_c}{I_\lambda^{in}} - 1\right)(1 - e^{-\tau_\lambda}), \tag{3}$$

where I_c is continuum intensity. The data of $\frac{I_\lambda^{in}}{I_c}$ were adopted from Wallace et al. (1993) for near-infrared wavelengths and Wallace et al. (1998) for visible wavelengths (See Figure 1.).

The source function, S_λ, depends on incident intensity (I_λ^{in}) from the background and on the way of redistribution. Insofar as the way of redistribution is concerned, this source function can be thought to be a result either of complete redistribution(CRD) or coherent scattering or partial redistribution(PRD) which is a mixture of CRD and coherent scattering. Theoretically, CRD is known to be the most suitable for Hα and Ca II line core (Vardavas 1974), in which case the source function is independent of wavelength. Note that the CRD is applicable within a wavelength range of 3 or 4 of Doppler width (Thomas 1957, Vardavas 1974). Since we know that I_λ^{in} is close to the intensity at the line center ($I_{\lambda 0}$) within this range, we adopt the values $I_{\lambda 0}$ as references of S_λ.

If we assume that S_λ is mainly contributed by the scattering from background (photosphere), the source function of the cloud can be determined from the mean intensity of the background. In the case of Hα, $\frac{S_\lambda}{I_c}$ is about 0.08 (Heinzel 1994), which corresponds to $\frac{S_\lambda}{I_{\lambda 0}} = 0.5$ (Heinzel 2006). This is physically reasonable, because roughly half side of a filament is illuminated by the light from the photosphere. Since the same argument may be applicable to Ca II lines, we will adopt this ratio to the Ca II lines. That is, we assume that the source function is half of the line center intensity for Ca II lines as well as Hα.

Therefore, the source function can be expressed as follows

$$S_\lambda = aI_c = bI_{\lambda 0}, \tag{4}$$

where $I_{\lambda 0}$ indicates intensity at the line centers, and we adopt $b = \frac{1}{2}$ (Heinzel 2006).

Finally, this yields another form of contrast equation

$$C_\lambda = \left(a\frac{I_c}{I_\lambda^{in}} - 1\right)(1 - e^{-\tau_\lambda}) = \left(b\frac{I_{\lambda 0}}{I_\lambda^{in}} - 1\right)(1 - e^{-\tau_\lambda}). \tag{5}$$

To determine τ_λ for a single velocity thread, we assume a Gaussian profile

$$\tau_\lambda = \tau_0 e^{-\left(\frac{\lambda - \lambda_D}{\Delta\lambda_D}\right)^2}, \tag{6}$$

where λ represents the wavelength measured from the line center, λ_D is the Doppler shift of the spectral line due to the bulk motion, and $\Delta\lambda_D$ is the Doppler width given by

$$\Delta\lambda_D = \frac{\lambda}{c}\sqrt{\frac{2kT}{m} + \xi^2}, \tag{7}$$

where m is the mass of an element which emits the spectral line and ξ is non-thermal turbulent velocity.

If multiple velocity threads exist along the line of sight (e.g., red-shifted, blue-shifted, stationary), the total optical thickness τ_λ can be represented as

$$\tau_\lambda = \tau_r e^{-\left(\frac{\lambda - \lambda_r}{\Delta\lambda_D}\right)^2} + \tau_s e^{-\left(\frac{\lambda}{\Delta\lambda_D}\right)^2} + \tau_b e^{-\left(\frac{\lambda - \lambda_b}{\Delta\lambda_D}\right)^2}, \tag{8}$$

where λ_r and λ_b stand for the shifts of line components due to the bulk motion of filaments/prominences, respectively.

III. RESULT

(a) Single Component Case

Assuming that there exists a single velocity thread along the line of sight, we have simulated spectral profiles of spectral lines - Hα, Ca II 8542, and Ca II K.

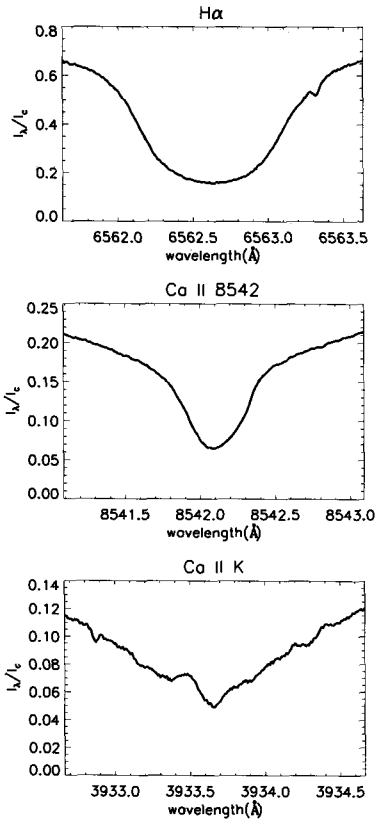

Fig. 1.— $\frac{I_\lambda^{in}}{I_C}$ of each spectral line (Wallace et al. 1993, Wallace et al. 1998). Two Ca II lines have less values at the line centers than Hα. This can result in more noise levels in terms of contrast profiles.

This thread is assumed to have proper Doppler motion. From this simulation, we could construct 1) contrast profiles at the disk filament, 2) absorption intensity profiles from the disk filament, 3) emission intensity profiles from the limb prominence. By comparing these results, we will be able to choose the spectral line which is the most advantageous in discriminating filaments/prominences from background.

Since many physical parameters of filaments/prominences are required to draw a spectral profile, we have set these values based on literatures and observations. For example, to define Doppler widths of a velocity thread, we have adopted typical physical parameters for filaments/prominences (T=8500K, ξ= 4km/s). And to determine Doppler shift (λ_D) and optical thickness at the line center of Hα and Ca II 8542 ($\tau_{0H\alpha}$, τ_{08542}), we have referred to the spectral profiles from observations (Tziotziou et al. 2001, Molowny-Horas et al. 1999). In the case of finding $\tau_{0H\alpha}$ and τ_{08542}, a fitting method has been applied to match our model with these observation profiles. To find out optical thickness of Ca II K (τ_{0K}), we have referred to several observations (Gouttebroze, Vial, & Heinzel 1997, Kubota 1980) which gave information on the ratio of emission energy (integrated line intensity) between Ca II 8542 and Ca II K ($E_K = 10E_{8542}$). Note that under the optically thin approximation, the integrated line intensity is proportional to the product of center optical depth, Doppler width and the source function.

Considering all these constraints, we have constructed contrast profiles of disk filaments and intensity profiles for filaments/prominences in Figure 2. The result of determining Doppler velocity and optical thickness of each spectral line center was $\tau_{0H\alpha}$ =0.91, τ_{08542}=0.52, τ_{0K}= 6.6 and Doppler velocity deduced from λ_D = -0.94km/s.

In all the spectral lines, contrasts near line center show negative values, which means that filaments are darker than background. Also, we can expect that Ca II 8542 may show less contrast than Hα, which is consistent with observation (Tziotziou et al. 2001; Molowny-Horas et al. 1999), while Ca II K may have higher distinction than Hα and Ca II 8542. Limb prominences also show that Ca II 8542 is expected to emit much less intensity than Hα and this tendency is consistent with observation (Stellmacher, & Wiehr 2000), while the intensity of Ca II K is comparable to Hα.

(b) Distinguishing Bulk Motion Components

We tried to construct spectral profiles in the case of multi-velocity threads. According to Chae et al. (2007), dynamic threads may be typically modeled by a superposition of three velocity components which have Doppler velocities of -15km/s, 0km/s, 15km/s and optical thickness ratio of 1:2:1, respectively. Adopting the optical thicknesses of single component case, the optical thickness values of our model cloud are 0.46, 0.91,0.46 in Hα, 0.26, 0.52, 0.26 in Ca II 8542, and 3.3, 6.6, 3.3 in Ca II K, respectively. Using this configuration, we have plotted spectral profiles for the same spectral lines in Figure 3.

As we see in Figure 3, Hα is a poor indicator to resolve Gaussian components with proper bulk motions. In Ca II lines, on the other hand, red-shifted and blue-shifted components seem to be easily identified. It is mainly due to small Doppler width of Ca II, because Ca ions have heavier mass than hydrogen atoms.

(c) Instrumental Photon Count

To record dual-band spectra, we adopted two identical imaging CCD cameras – ixon DV887 of ANDOR Technology. This has a frame rate of 32~263fps, which is suitable for fast imaging. Its main specifications are described in Table 1.

One of the purposes of this study is to estimate the photon count from filaments/prominences for each spectral line, so that we can suggest the proper exposure time for any required signal-to-noise (S/N) ratio. Since the biggest source of noise originates from Poisson noise and readout noise ($N_R = \frac{62e^-}{M}$, full frame with a readout rate of 10MHz, where M is multipli-

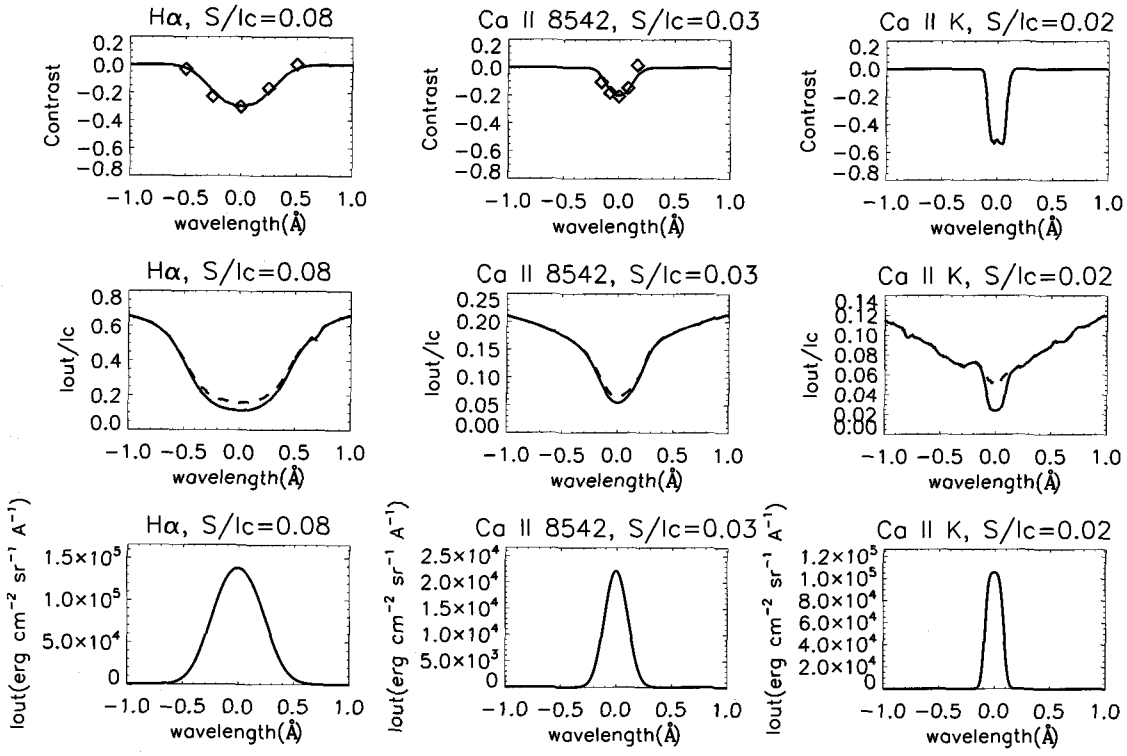

Fig. 2.— Expected spectral profiles for single component case. Top: Contrast profiles of disk filaments(solid) compared to the observation data(diamond) taken by Tziotziou et al. (2001) and by Molowny-Horas et al. (1999), Middle: Intensity profiles of disk filaments(solid) with intensity from the photosphere(dashed), Bottom: Intensity profiles of limb prominences

TABLE 1.
SPECIFICATION OF IXON DV887

Parameters	Values
Active pixels	512x512
Pixel size(μm)	16x16
Image area(mm)	8.2x8.2
Active area pixel well depth	220,000 e^-
Gain register pixel well depth	800,000e^-
Max readout rate	10MHz
Frame rate	32~263fps
Readout noise	< 1~62 at 10MHz
Electron multiplier gain	1~1000
Digitization at 10MHz	14bit
Dark current	0.5e^-/pix/sec

cation factor of electron-multiplying CCD (EMCCD) method), it is important to know photon count for an exposure.

There are many factors which contribute to the photon count. The photon (electron) count at the continuum (N_e) may be expressed as follows;

$$N_e = q\tau_{atm}\tau_{ins}\frac{I_C}{h\nu}\Delta\Omega\Delta\lambda\Delta A\Delta t \tag{9}$$

$$= q\tau_{atm}\tau_{ins}I_C\frac{\lambda}{hc}\Delta x\Delta y\frac{\pi}{4F^2}\Delta\lambda\Delta t. \tag{10}$$

The definitions of the factors and their values are described in Table 2.

In addition, we can determine S/N values of filaments/prominences from N_e. If we are to measure contrast of disk filaments, it is meaningful to calculate S/N of contrast. In this case, S/N can be represented as follows

$$S/N = \left|\frac{C_\lambda}{\delta C_\lambda}\right| = \left|\frac{\frac{N_\lambda^{out}-N_\lambda^{in}}{N_\lambda^{in}}}{\frac{\delta N_\lambda^{out}}{N_\lambda^{in}}}\right| = \left|\frac{N_\lambda^{out}-N_\lambda^{in}}{\sqrt{N_\lambda^{out}+N_R^2}}\right|, \tag{11}$$

where $N_\lambda^{in} = N_e\frac{I_{in}}{I_c}$, $N_\lambda^{out} = N_e\frac{I_{out}}{I_c}$ implying photon count from background and filaments, respectively, and $N_R = \frac{62e^-}{M}$.

In the case of limb prominences, we can calculate S/N of photon count directly

$$S/N = \frac{N_\lambda^{out}}{\delta N_\lambda^{out}} = \frac{N_\lambda^{out}}{\sqrt{N_\lambda^{out}+N_R^2}}. \tag{12}$$

The estimation of S/N for filaments/prominences are shown in Figure 4.

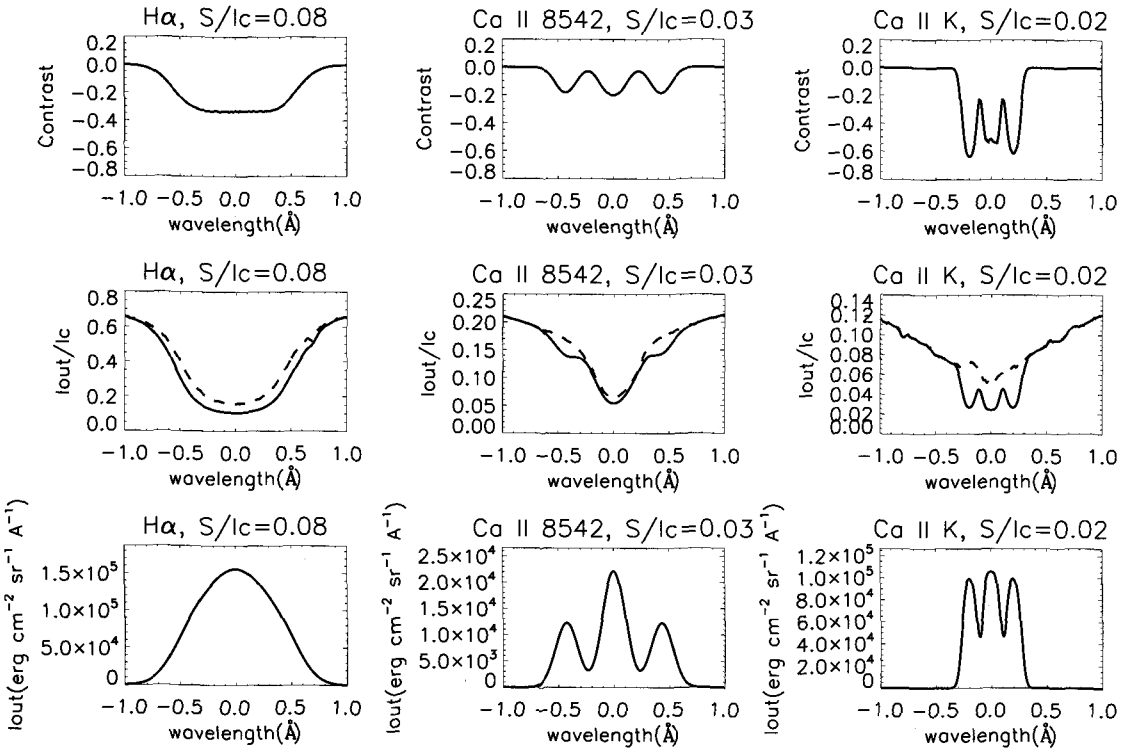

Fig. 3.— Expected spectral profiles for multi component case. Top: Contrast profiles of disk filaments, Middle: Intensity profiles of disk filaments(solid) with intensity from the photosphere(dashed), Bottom: Intensity profiles of limb prominences

As seen from Figure 4, Ca II has weaker signal-to-noise ratios than Hα. This is mainly because the values of the source function in Ca II lines are low, which are regarded to be strongly coupled with intensity at the line centers.

As it is well known, the S/N value increases if we take a longer exposure time. In this case, it is not desirable because it limits fast imaging feature of the spectrograph. Instead, if we utilize electron-multiplying CCD (EMCCD) method, S/N can be enhanced due to lower readout noise.

Then, let us estimate optimum camera parameters to make S/N ratio as high as possible. Within the limit of pixel well depths (220,000e^- for active area, 800,000e^- for gain register) and maximum ADU count (2^{14}=16,384), we can adjust gain and electron multiplication. Maximum multiplication factors (M) have been selected so as to fill up gain register pixel well (800,000e^-). In this case, we only considered the intensity near the line centers (-1Å< λ < +1Å) and brightening of filaments/prominences has been ignored. Due to fast image scanning purpose, exposure time has been set as 0.02s. The suggested parameters are shown in Table 3. and Table 4. As seen from these tables, EMCCD is helpful to increase S/N values, because in these cases readout noises ($\frac{62e^-}{M}$) are comparable to Poisson noises, which are caused by the electron counts themselves.

IV. DISCUSSION

We have deduced parameters like optical thickness from the data given in previous observational studies (Tziotziou et al. 2001, Molowny-Horas et al. 1999). The question is then whether these parameters would be suited for FISS which will have higher spatial resolution and higher spectral resolution than these observations. There is a concern that the adopted optical thickness (0.91 in Hα) may be overestimated.

A single thread would appear blurred in low resolution observations, resulting in low contrast and small optical thickness. In this case, high resolution observations will yield higher contrast and larger optical thickness. This seems to be the case that is observed in high spatial resolution images (Lin et al. 2004).

What if not a single thread, but a bundle of threads are observed? What is important is the spatial distribution of the threads. One extreme case is when all the threads are along the line of sight. In this case, the average optical thickness of each thread should be equal to our value (e.g, 0.91) divided by the number of threads. According to several previous studies (Engvold et al. 1989, Mein & Mein 1991, Mein et al. 1994, Chae et al. 2007), the number of velocity threads along the line of sight in previous observations ranges from 3

TABLE 2.
LINE-SPECIFIC AND COMMON VALUES TO CALCULATE N_e

Parameter	Name	Hα	Ca II 8542	Ca II K
q	quantum efficiency at the CCD	0.9	0.55	0.5
τ_{atm}	atmospheric transmissivity	0.699	0.706	0.423
$\Delta\lambda$ (Å)	spectral coverage of a pixel	0.028	0.046	0.017
I_C	Intensity of continuum (erg · cm^{-2} str^{-1} sec^{-1} Å^{-1})	2.9×10^6	1.78×10^6	4.41×10^6
N_e	photon count of continuum	2.51×10^5	2.03×10^5	4.67×10^4
τ_{ins}	instrumental transmissivity		0.25	
Δx	physical width of a CCD pixel		16μm	
Δy	physical height of a CCD pixel		16μm	
Δt	exposure time		0.02s	
F	focal ratio of incident beam at the entrance slit of FISS		26	

to 6, and each thread has an optical thickness of from 0.2 to 0.3. The number of density threads may be even bigger and the optical thickness of a density may be even smaller, since each velocity thread may consist of several density threads. When several threads are along the line of sight, the integrated effect of threads may be incorporated by including more terms in equation (8). The cloud model in equations (2) and (3) critically depend on the assumption of the constant source function, which may be valid unless the integrated optical thickness is much bigger than unity.

On the other hand, we note one important aspect of high spatial resolution. That is, the line of sight is more strictly defined than in low resolution observations so that the line of sight may contain less threads. Namely, the effect of line-of-sight overlapping will be reduced in high resolution observations. It would be quite interesting to see how the velocity threads and density threads would be observed with FISS having high spatial resolution.

If we apply the cloud model to the observational data taken by Tziotziou et al. (2001) and Molowny-Horas et al. (1999), we find that optical thickness of Hα (0.91) and Ca II 8542 (0.52) are in the same order of magnitude, yielding ratio of $\frac{\tau_{DH\alpha}}{\tau_{D8542}} = \frac{1.75}{1}$. That is why the two spectral line profiles show similar contrast values.

However, in general, the ratio may differ from region to region. According to Stellmacher (2000), the ratio of integrated intensity between Ca II 8542 and Hβ differs among individual prominences. The study compared two prominences - a bright prominence and a faint one. The ratio of $\frac{E_{8542}}{E_{H\beta}}$ ranges from 0.28 for the bright prominence to 0.63 for the faint one. And $\frac{E_{H\alpha}}{E_{H\beta}}$ was between 6 and 12 for the bright prominence. This implies that $\frac{E_{H\alpha}}{E_{8542}}$ also does not have a fixed value but has a range. On average, the ratio of $\frac{E_{H\alpha}}{E_{8542}}$ was approximately 30. If we assume that the prominences are optically thin, so that optical thickness is proportional to intensity and if we consider the ratio of Doppler width for Hα and Ca II 8542 as $\frac{\Delta\lambda_{DH\alpha}}{\Delta\lambda_{D8542}} = \frac{27}{13}$, the estimated ratio of optical thickness is about $\frac{\tau_{DH\alpha}}{\tau_{D8542}} = \frac{3.3}{1}$, which is differ from our expectation.

The discrepancy in terms of optical thickness ratio may signify that the temperature of filament threads varies from region to region. Since most of filaments/prominences have arc shapes in the chromosphere, they can be exposed to different temperatures. Usually, the higher chromosphere region has a higher temperature. So this can change the ratio of Hα absorbers to Ca II 8542 absorbers. The lower energy level of Ca II 8542 is 1.69eV from the ground and the lower level of Hα is 10.6eV. Therefore, in the high chromosphere region, the number density of electrons which contribute to Ca II 8542 can decrease considerably due to excitation to upper levels. On the other hand, the lower chromosphere region can have abundant Ca II 8542 absorbers/emitters. Figure 7 of Tziotziou et al. (2001) supports such an explanation. The lower region (barbs) of the filament look thicker than the central parts in Ca II 8542, but the filament in Hα does not seem to have much variation along it.

Therefore, it is possible for the two spectral lines to see different heights of filaments/prominences. That can be a reason for Ca II 8542 to be prominent near the barbs, since it has lower energy level than Hα. Wang et al. (1998) gives a good insight for that. Figure 1 of this paper shows that Hα and He II 304 Å are emitted from different regions in filaments/prominences. The higher region where He II 304 is intense has a weak emission from Hα. On the contrary, lower chromosphere has a strong Hα emission while He II 304 is faint. This is mainly because the emissivity of He II 304 peaked near the temperature of 80,000K, while Hα is strong near 10,000K. The temperatures correspond to the energy level where the electrons are abundant. He II 304 has a higher energy level than Hα. Since filaments/prominences can have both low and high temperatures, the higher region of filaments/prominences

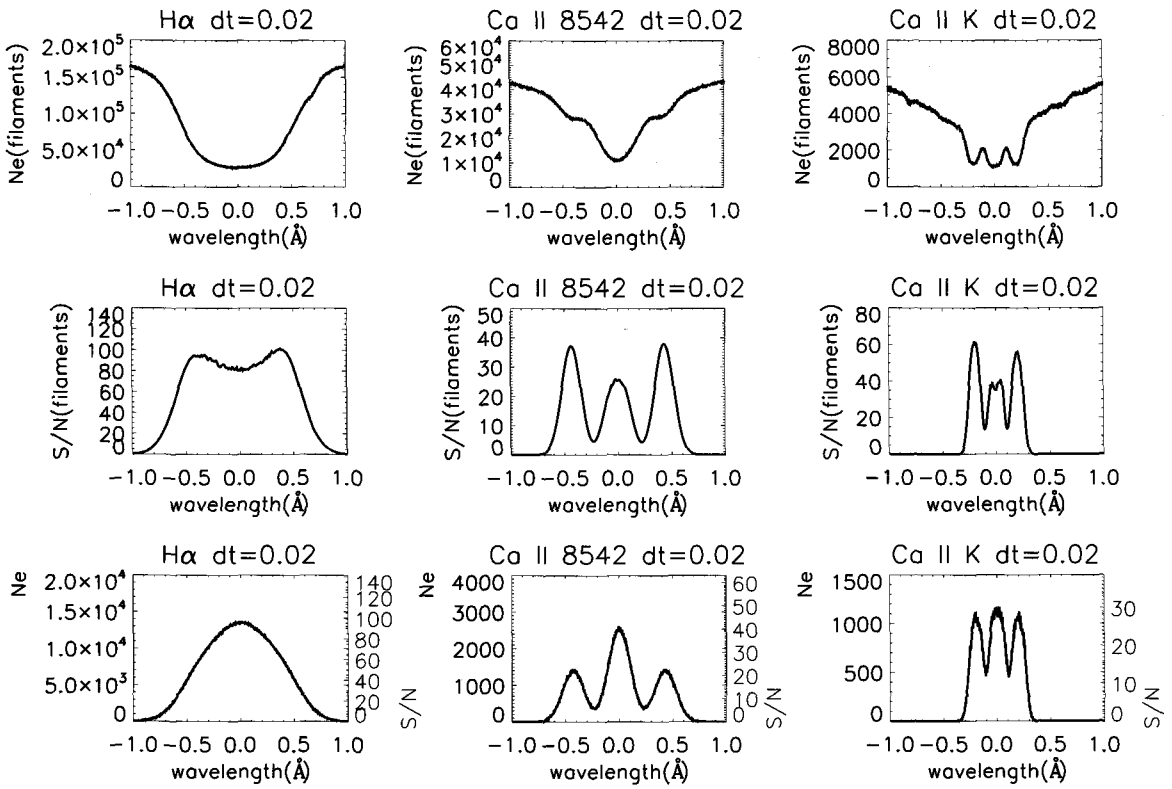

Fig. 4.— Expected photon count and corresponding signal-to-noise ratio. Top and middle : Photon count and signal-to-noise ratio in the case of observing filaments at the disk center. Bottom: Photon count and signal-to-noise ratio in the case of observing prominences at the limb. Exposure time is 0.02s.

will be prominent in He II 304, middle region in Hα, and low region in Ca II 8542.

Our consideration on the relative intensity above is based on previous observations that did not resolve threads. It would be also interesting to see how the ratio varies from thread to thread using high spatial resolution observations.

Finally, let's think about the validity of the CRD assumption we used. It is known to be valid within a wavelength range of $3 \sim 4|\Delta\lambda_D|$. With this assumption, the intensity of line center may be used to derive the source function of fine threads within this wavelength range. It may be appropriate for stationary components to choose line center intensities as a reference of source function, since spectral coverage of the threads is within this range. In the case of moving threads, if we refer to typical bulk motion speed of the threads, the wavelength coverage may be out of $3 \sim 4|\Delta\lambda_D|$ from line center. Nevertheless, we have referred to line center intensities for all the components, because the intensities at the Doppler-shifted wavelength do not deviate much from that of line center. We can still apply constant source function regardless of wavelength (CRD).

V. CONCLUSION

The purpose of this study is to estimate the spectral line profiles of filaments/prominences in the spectral lines Hα, Ca II 8542, and Ca II K. Instrumental specifications of NST/FISS have been considered to calculate photon count and to determine optimal exposure time for each line.

We expect that it will be possible to estimate temperature and non-thermal turbulence through simultaneous recording of two spectral lines using dual cameras. We also expect that it will be possible to study fine structures of filaments/prominences by observing Ca II spectra. According to our study, there is much possibility of detecting multi-velocity threads in filaments/proiminences. For this purpose, we have predicted the optimal parameters of NST/FISS to fulfill our needs for good data quality. What should be done from now on is to verify our prediction from real observations using NST/FISS.

ACKNOWLEDGEMENTS

We appreciate the referee's constructive comments. This work was supported by the Korea Research Foundation Grant (KRF-2002-015-CS0020).

TABLE 3.
OPTIMAL CAMERA CONTROL PARAMETERS FOR MAXIMUM S/NS IN THE CASE OF FILAMENTS.
EXPOSURE TIME : 0.02S.

parameter	Hα	Ca II 8542	Ca II K
Maximum electron count at $\pm$1Å (e^-)	166,000	43,600	5,770
Line center photon count (e^-)	26,300	10,900	1,060
Maximum multiplication factor	4	18	138
Gain (e^-/ADU)	40	47	48
Maximum S/N	101	37	62

TABLE 4.
OPTIMAL CAMERA CONTROL PARAMETERS FOR MAXIMUM S/NS IN THE CASE OF PROMINENCES.
EXPOSURE TIME : 0.02S.

parameter	Hα	Ca II 8542	Ca II K
Line center photon count (e^-)	13,700	2,630	1,200
Maximum multiplication factor	58	304	666
Gain (e^-/ADU)	1	1	1
Maximum S/N	117	51	34

REFERENCES

Beckers, J. M., 1964, Ph.D. Thesis, University of Utrecht (AFCRL-Environmental Research Paper, No.49)

Chae, J., Park, H.-M., & Park, Y.-D., 2007, Hα Spectral Properties of Velocity Threads Constituting a Quiescent Solar Filament, JKAS, 40, 67

Choi, S., Kim, Y.-H., Moon, Y.-J., Cho, K.-S., Park, Y.-D., Jang, B.-H., Kim, S.-J., & Kim, K.-S., 2005, Component-Based Development of Observational Software for KASI Solar Imaging Spectrograph, JKAS, 38, 463

Denker, C., Goode, P. R., Ren, D., Saadeghvaziri, M. A., Verdoni, A. P., Wang, H., Yang, G., Abramenko, V., Cao, W., Coulter, R., Fear, R., Nenow, J., Shoumko, S., Spirock, T. J., Varsik, J. R., Chae, J., Kuhn, J. R., Moon, Y., Park, Y. D., & Tritschler, A., 2006, Progress on the 1.6-meter New Solar Telescope at Big Bear Solar Observatory, SPIE, 6267, 10

Engvold, O., Malville, J. M., & Livingston, W., 1978, The Fine Structure of Prominences, SoPh, 60, 57

Engvold, O., Jensen, E., Zhang, Y., & Brynildsen, N., 1989, Distribution of Velocities in the Pre-Eruptive Phase of a Quiscent Prominence, HvaOB, 13, 205

Goode, P. R., Denker, C. J., Didkovsky, L. I., Kuhn, J. R., & Wang, H., 2003, 1.6 M Solar Telescope in Big Bear – The NST, JKAS, 36,S1, S125

Gouttebroze, P., Vial, J.-C., & Heinzel, P., 1997, Formation of Ca II Lines in Solar Prominences, SoPh, 172, 125

Heinzel, P., Gouttebroze, P., & Vial, J.-C., 1994, Theoretical Correlations between Prominence Plasma Parameters and the Emitted Radiation, A&A, 292, 656

Heinzel, P. & Anzer, U., 2006, On the Fine Structure of Solar Filaments, ApJ, 643, L65

Kubota, J., 1980, The Optical Thickness of Quiescent Prominences in the Ca II K Lines and the Centeral Reversal in the Spectral Lines, PASJ, 32, 359

Lin, Y., Engvold, O., van der Voort, L. R., Wiik, J. E., & Berger, T. E., 2005, Thin Threads of Solar filaments, SoPh, 226, 239

Mein, P. & Mein, N., 1991, Dynamical Fine Structure of a Quiescent Prominence, SoPh, 136, 317

Molowny-Horas, R., Heinzel. P., Mein, P., & Mein, N., 1999, A non-LTE Inversion Procedure for Chromospheric Cloud-like Features, A&A, 345, 618

Schmieder, B., 1992, Structural Elements of Filaments, SoPh, 141, 275

Stellmacher, G. & Wiehr, E., 1973, Observation of an Instability in a "Quiescent" Prominence, A&A, 24, 321

Stellmacher, G. & Wiehr, E., 2000, Two-dimensional Photometric Analysis of Emission Lines in Quiescent Prominences, SoPh, 196, 357

Tandberg-Hanssen, E., 1995, The Nature of Solar Prominences, Kluwer Academic publishers

Thomas, R. N., 1957, The Source Function in a Non-equilibrium Atmosphere. I. The Resonance Lines, ApJ, 125, 260

Tziotziou, K., Heinzel, P., Mein, P., & Mein, N., 2001, Non-LTE Inversion of Chromospheric Ca II Cloud-like Features, A&A, 366, 686

Tziotziou, K., 2007, Chromospheric Cloud-Model Inversion Techniques, ASPC, 368, 217

Vardavas, I. M. & Cram, L. E., 1974, Partially Coherent Scattering Models for the Formation of the Chromospheric Ca II K Line, SoPh, 38, 367

Wallace, L., Hinkle, K., & Livingston, W. C., 1993, An Atlas of the Photospheric Spectrum from 8900 to 13600 cm(-1) (7350 to 11230 [angstroms]), National Solar Observatory

Wallace, L., Hinkle, K., & Livingston, W., 1998, An Atlas of the Spectrum of the Solar Photosphere from 13,500 to 28,000 cm-1 (3570 to 7405 A), National Optical Astronomy Observatories

Wang, H., Chae, J., Gurman, J. B., & Kucera, T. A., 1998, Comparison of Prominences in Hα and He II 304Å, SoPh, 183, 91

Zhang, Q. Z. & Fang, C., 1987, Semi-empirical Models of a Quiescent Prominence, A&A, 175, 277

Zhang, Q. Z., Livingston, W. C., Hu, J., & Fang, C., 1987, Spectral Analysis and the Two-dimensional Dstribution of Physical Parameters in a Quiescent Prominence, SoPh, 114, 245

Zirker, J. B. & Koutchmy, S., 1990, Prominence Fine Structure, SoPh, 127, 109

Zirker, J. B. & Koutchmy, S., 1990, Prominence Fine Structure. II - Diagnostics, SoPh, 131, 107